Crystallographic reorientation and nanoparticle coalescence

R. Theissmann,[1,2,3] M. Fendrich,[4] R. Zinetullin,[4] G. Guenther,[5,3] G. Schierning,[1,2,3] and D. E. Wolf[4,2,*]
[1]*Faculty of Engineering, University of Duisburg-Essen, Bismarckstr. 81, 47057 Duisburg, Germany*
[2]*CeNIDE, University of Duisburg-Essen, 47057 Duisburg, Germany*
[3]*Institute of Nanotechnology, Forschungszentrum Karlsruhe GmbH, 76021 Karlsruhe, Germany*
[4]*Department of Physics, University of Duisburg-Essen, Lotharstr. 1, 47057 Duisburg, Germany*
[5]*Material Science and Engineering, Darmstadt University of Technology, Petersenstr. 23, 64287 Darmstadt, Germany*
(Received 5 February 2008; revised manuscript received 21 August 2008; published 10 November 2008)

Complementary experimental and theoretical results on the coalescence of nanoparticles demonstrate the importance of the crystallographic orientation on the coalescence process. *In situ* hot-stage transmission electron microscopy studies on self-supporting films consisting of indium tin oxide nanoparticles clearly show rotations of neighboring particles preceding their coalescence. Both rotation and coalescence are observed well below half the melting temperature. The coalescence of two adjacent nanoparticles is simulated by means of a combination of the kinetic Monte Carlo method for atomic diffusion with an integration of the equations of motion for the rigid body degrees of freedom of the two particles. This allows analyzing the reorientation of the two crystal lattices prior to the merging process. Thus, nanoparticle coalescence has theoretically as well as experimentally been shown to be a two-step process: first a reorientation of adjacent nanoparticles, and second their complete or incomplete coalescence depending on the matching of the crystallographic orientations.

DOI: 10.1103/PhysRevB.78.205413 PACS number(s): 68.35.Fx, 68.37.Og, 61.46.Bc, 61.72.Mm

I. INTRODUCTION

Nanopowders are crucial for many new technical developments in catalysts, fuel cells, gas sensors, thermoelectrics, and other devices. The functionality (e.g., mechanical stability or conductance) of these powders can be improved by a certain degree of sintering, but too much of it may lead to the loss of nanoscale features.[1–3] The goal of the investigations presented here is to develop strategies to control the initial stage of the sintering process and to suppress its negative late stage implications.

Traditional models[4,5] regard sintering as one continuous process: At about 2/3 of the melting temperature thermally activated processes such as surface- and grain-boundary diffusion of atoms become fast enough to cause noticeable morphology changes of a nanopowder. Solid necks grow between the particles, stabilizing the agglomerate mechanically. This process is capillary driven, i.e., it reduces the surface free energy.

In principle the reduction in free energy would ultimately lead to the complete coalescence of the particles into a single crystal. In practice, however, this is usually kinetically preempted by local free-energy minima surrounded by high barriers. An important example was given by Kellett and Lange,[6,7] who showed that the presence of grain boundaries between the particles may suppress pore shrinkage completely once the equilibrium contact angles are reached. A further lowering of the free energy would require the recrystallization of some particles in order to remove some of the grain boundaries.

Indeed, thin granular metallic films heated *in situ* in the transmission electron microscope (TEM) or scanning electron microscope (SEM) have shown that sometimes grains suddenly reorient upon heating. Such discontinuous grain rotations seem to contribute to the development of the microstructure during annealing.[8–11]

Therefore, atomistic models describing the process of coalescence must account for changing crystallographic mismatch. A convenient way to characterize crystallographic constellations is the coincident site lattice (CSL) model.[12] This model assumes that only certain relative orientations of the constituting lattices are favorable, namely, those exhibiting a large fraction $1/\Sigma$ of lattice points exactly coinciding in space. Obviously Σ has only odd values, $\Sigma=1,3,5,\ldots$. $\Sigma=1$ means an identical orientation of both lattices, and twin-boundary constellations have $\Sigma=3$.

In order to investigate reorientation during sintering, many groups have performed the following type of experiments ("crystallite rotation technique"): A small single-crystalline particle is placed with random misorientation on top of a well-characterized single-crystalline surface. During an annealing procedure, the particle can reorient. The resulting orientations and grain boundaries between particles and substrate can in turn be analyzed statistically. It is assumed that the crystallites rotate into the nearest configuration, which corresponds to a local minimum of the grain-boundary energy. With sufficient statistics, the main minima of the grain-boundary energy can be identified.

Chan and Baluffi studied twisted Au particles on a Au layer: Au particles were grown epitaxially on a (001)-oriented NaCl single crystal, and a (001)-oriented Au-thin film was obtained similarly on a stack of NaCl and Ag. Those two pieces were welded together resulting in statistically twisted (001) particles on a (001) substrate. After annealing, the orientations of the particles were analyzed by *ex situ* TEM. Only twist rotations had occurred. They resulted in interfaces of mainly the types $\Sigma=1$ and $\Sigma=5$. With less occurrence also $\Sigma=13$, $\Sigma=17$, and a "near" $\Sigma=27$ could be identified. The mechanism of rotation included the motion of screw dislocations.[13] In a second paper, tilt boundaries and mixed boundaries were observed. The climbing of edge grain-boundary dislocations was identified as the main

mechanism for the thermally induced untilting or untwisting.[14]

Yeadon *et al.*[15] deposited initially randomly oriented, single-crystalline copper particles of the size of 4 nm to 20 nm onto 40-nm-thick (001)-oriented copper thin films and investigated the sintering *in situ* by hot-stage TEM. Heating the sample up to 250 °C, the smaller particles (5 nm to 10 nm) began to reorient, monitored by bright field and dark field contrast. Quickly the particles' contrast disappeared so that it was concluded that they had been consumed completely by the oriented thin film. It was suggested that the boundary would, at a certain point, move through the particle and, thus, be eliminated.

Bording *et al.*[16] investigated the size- and shape-dependent orientation of Ag nanocrystals on an epitaxial Si(111)-H surface both by molecular-dynamics (MD) simulations and experimentally. The simulation results showed that the orientation of the Ag nanocrystals after annealing was determined by the global minimum of the interface energy. For Ag particles with a large contact area the interface energy was mostly determined by interface atoms in complete CSL cells. If the contact area was small, the atoms in incomplete CSL cells induced large fluctuations in the preferred orientations, as observed also experimentally.

A corresponding MD simulation was carried out by Ashkenazy *et al.*[17] They generated statistically twisted platinum particles on a platinum surface. The observed rotations were spontaneous instead of thermally activated. Particles with a neck diameter below 5 nm, which one could regard as "not sintered," showed rotations. Particles bigger than the 5 nm did not.

The coalescence of two gold nanoparticles was studied by MD simulation by Arcidiacono *et al.*[18] During neck formation, small relative rotations of the particles were observed. The coalescence of two copper nanoparticles of approximately 5-nm diameter was simulated using MD at 700 K by Zhu and Averback.[19] A combination of elastic deformation and a relative rotation forming a twin boundary between the two particles was found.

All of the quoted literature on particle reorientation has in common that metals were investigated. The mechanism of reorientation may then include the formation or migration of grain-boundary dislocations. An overview over the role of line defects in metal-metal boundaries is given by Baluffi *et al.*[20]

But how do the details of coalescence between oxide particles look like? Here, the formation or movement of dislocations is virtually impossible. Studies of Rankin and Sheldon address the *in situ* TEM sintering of nanosized, single-crystalline ZrO_2. The particles were deposited onto an amorphous layer so that the free reorientation of the particles in space was partly hindered. At 1160 K, a reorientation of unconstrained ZrO_2 particles, which were in contact with only one other particle was observed.[21,22]

The focus of our work is a quantitative understanding of the correlation between crystallographic orientation and coalescence dynamics of oxide nanoparticles. By combining simulations based upon a simplified atomic model and *in situ* TEM it is shown that the investigated nanoparticles must adopt a suitable orientation by rotational and translational movements before coalescence takes place. If reorientation is suppressed, the lattice mismatch opposes the complete coalescence, in agreement with the predictions of Kellett and Lange.[6]

The experiments are designed such that initially indium tin oxide (ITO) particles, $In_2O_3:Sn^{4+}$, of random orientation form a loose, weakly agglomerated layer. The particles have only very small contact areas. In contrast to the crystallite rotation technique, the interfaces obtained by annealing were not predefined by a substrate orientation.

The theoretical part of our study deals with two randomly oriented particles, which may freely move and rotate against each other when in loose contact. The impact of their relative orientation on the ongoing coalescence is investigated systematically.

II. METHODS

A. Simulation

The early stages of neck growth, sintering, and coalescence of particle agglomerates are far from universal: They depend on the material, the preparation history of the agglomerate, on the crystallinity of the particles, and on their coupling to a heat bath, just to name a few influencing factors. In order to investigate specific mechanisms at work it is helpful to use simplified models, but one must carefully specify the key properties of the agglomerates such a model intends to describe.

The simulation part of this paper deals with a simple model characterized by the following key properties: All particles consist of the same crystalline material, which is assumed to be sufficiently hard so that plastic deformation and dislocation activities can be neglected. Initially the particles are assumed to be approximately spherical. Their interaction should be short range.

When such hard, round particles come into first contact at low temperature, they stick together only weakly because no solid bridge has formed between them yet. One calls this a soft agglomerate because the particles can easily roll on each other, and can even be separated again, e.g., by thermal fluctuations or turbulent shear forces in a dispersion. However, once a sinter neck has formed, the connection between the particles is rigid. One calls this a hard agglomerate.

The purpose of our model is to investigate the transition from a soft to a hard agglomerate, which in turn can lead to complete coalescence under favorable conditions. This requires atomic diffusion, which is assumed to take place predominantly at the particle surfaces and along the grain boundaries in between neighboring particles of different crystallographic orientations. Temperature is assumed to be constant.

In addition to atomic diffusion, rigid body motion of the particles as a whole turns out to be important. For example the particles can "roll" on each other, thereby altering their crystallographic orientation. In order to take atomic diffusion and particle reorientation into account simultaneously, a hybrid simulation technique has been developed, which we describe in detail below. It combines kinetic Monte Carlo (KMC) steps[23,24] for the atomic diffusion with the numerical

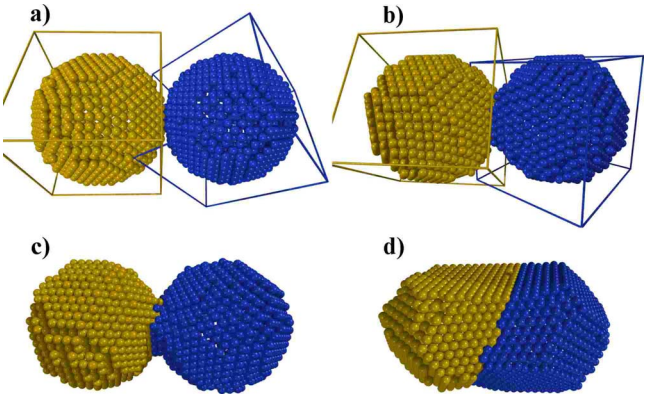

FIG. 1. (Color online) Snapshots of simulated evolution. The two colors indicate to which lattice the atoms belong. Perspective cuboid axes indicate the $\langle 111\rangle$, $\langle 1\bar{1}0\rangle$, and $\langle 11\bar{2}\rangle$ directions of the fcc lattices. (a) Initial configuration with two equally sized but randomly oriented nanoparticles brought into contact. (b) Crossover from the reorientation to the coalescence regime: The relative movement has frozen in at a certain Σ value. (c) A sinter neck has grown. (d) Final constellation with twin boundary. The simulation of the evolution from (a) to (b) is done using the hybrid simulation code. Once the orientation has frozen in, a pure KMC method is used for simulating the further sintering [images (c) to (d)]. The whole simulation process can be seen in Ref. 27.

integration of the equations of motion for the six rigid body degrees of freedom of each particle[25,26] ["rigid body dynamics" (RBD)].

These are the key features of the simulation model we propose. No further material properties will be taken into account. That these key features can be realized in an experimental system is demonstrated in the second part of this paper, which deals with (initially) soft agglomerates of hard, round, crystalline ITO particles.

1. Detailed description of the hybrid simulation technique

In the simulation model each particle of the agglomerate has an fcc lattice of its own, with individual orientation and position of the origin. The atoms belonging to a particle can only reside on these lattice sites. This excludes elastic deformation as well as topological crystal defects such as dislocations or stacking faults. Each lattice extends beyond the occupied region into free space and defines the possible sites to which the atoms of the corresponding particle may migrate.

In the following we restrict ourselves to the case of two particles. Generalization to larger agglomerates is straightforward. The initial configurations are generated as follows: All sites of an fcc lattice within a certain distance from the origin are filled by atoms, giving a compact (nearly) spherical particle. This particle is copied to obtain a second, independent particle. Then we randomly rotate both lattices and place their origins such that the particles just touch [see Fig. 1(a)].

A diffusion step takes an atom either to a free neighboring site of the same lattice or to a nearby free site of the other lattice. Surface diffusion dominates, but volume and grain-boundary diffusion occur as well. Simultaneously, each particle is allowed to move and rotate in space under the influence of forces and torques acting on it. Two different algorithms are combined to simulate the atomic diffusion on one hand, and the rigid body dynamics on the other hand. These algorithms and how they are combined will now be described in detail.

Atomic diffusion is simulated as a stochastic hopping process between neighboring binding sites by means of a KMC algorithm. The rates q of the individual processes are given by the Arrhenius law determined by the activation energies E_{act},

$$q = \nu_0 \exp\left(-\frac{E_{\mathrm{act}}}{k_{\mathrm{B}}T}\right) \tag{1}$$

with attempt frequency ν_0, temperature T, and Boltzmann's constant k_{B}.

All possible diffusion processes and their rates have to be known at any time. In each KMC step one particular process is chosen from the list at random with a probability q/Q, where Q is the sum of all rates. The chosen process is carried out, and time is incremented by

$$\Delta t_{\mathrm{KMC}} = -\frac{1}{Q}\ln\{\mathrm{Rnd}(0,1)\}. \tag{2}$$

The sum t_{KMC} corresponds to real time.[23]

A possible diffusion process leads from an occupied initial site to a nearby unoccupied site on either lattice, which must have at least two occupied nearest neighbors. If there are only two neighbor atoms, it is not a binding site but a saddle point. Then the atom is immediately moved on to a randomly chosen neighbor site exhibiting three or more direct neighbors.

In the case that the initial and the destination site belong to the same lattice, they must be nearest neighbors. Then the activation energy in our simulation model is defined by

$$E_{\mathrm{act}} = \begin{cases} E_0 + \max(0, E_{\mathrm{b,f}} - E_{\mathrm{b,i}}), & \text{for more than two final neighbors} \\ E_{\mathrm{b,f}} - E_{\mathrm{b,i}}, & \text{for exactly two final neighbors} \end{cases}, \tag{3}$$

where $E_{\mathrm{b,i}}(E_{\mathrm{b,f}})$ are the initial (final) binding energies. The parameter E_0 is related to a saddle-point energy in the following sense: Consider two neighboring binding sites with binding energies $E_{\mathrm{b,1}} < E_{\mathrm{b,2}}$ and saddle-point energy E_{S} in between. Then $E_0 = E_{\mathrm{S}} - E_{\mathrm{b,2}}$ is the activation energy for a hop from site 2 to site 1. The activation energy for the reverse hop is $E_{\mathrm{S}} - E_{\mathrm{b,1}} = E_0 + (E_{\mathrm{b,2}} - E_{\mathrm{b,1}})$. In other words, E_0 is the smaller one of the activation energies for hops back and forth between any two binding sites. The simplification of our model is that we assume that E_0 does not depend on the local atomic configuration. If applied to (111), respectively, (100) surfaces, this model would mean that one assumes both diffusion constants were equal.

For diffusion processes of atoms to a site on the other lattice, we have to address the fact that the hopping distance is no longer constant. We allow only distances between the starting and the destination site that do not exceed $1.5a$,

where a is the nearest neighbor distance on the fcc lattices. Assuming that energy barriers drop with decreasing hopping distance we approximate the local energy landscape by the radial parabolic potential $E(r)=E_b+\kappa r^2$. Given the initial site on one lattice and an allowed destination site on the other lattice, the saddle-point energy E_S between them is defined by the intersection of both sites' parabolas and, hence, depends on the distance between the minima. The activation energy is $E_{act}=E_S-E_{b,i}$. The parameter κ is determined by the requirement that simulation results should match if either a single-lattice model or two exactly coinciding lattices are used.

The second ingredient of our hybrid simulation scheme, the RBD, will be described now. Both particles are treated as rigid bodies. At first their centers of mass, as well as the tensors of their moments of inertia, are calculated. Next the total force exerted by the atoms of one particle on the atoms of the other one is evaluated, as well as the total torque. Finally the rigid translation and rotation of the particles is calculated by integrating the corresponding equations of motion. The modified velocity Verlet algorithm described in Ref. 25 is used with a time discretization $\Delta t_{RBD}=10^{-13}$ *s*. This defines a second time scale in our simulation with the total elapsed time t_{RBD}.

Both internal time scales are kept approximately synchronous in the following way: n KMC steps are performed one after the other as long as $t_{KMC}<t_{RBD}$. As soon as t_{KMC} gets ahead of t_{RBD}, m RBD steps are inserted, where $m=\lfloor(t_{KMC}-t_{RBD})/\Delta t_{RBD}\rfloor+1$. The values of n and m strongly depend on the used temperature. For the simulations presented in this paper n is mostly one and m varies between one and ca. 100 with an average of about nine. After each KMC step and at the ends of the RBD integration loops, the list of possible diffusion processes is updated.

2. Simulation parameters and procedure

We consider monatomic fcc crystals with a fixed nearest-neighbor distance a that serves as our length unit. The binding energies E_b of the atoms entering the activation energies, Eq. (3), as well as the forces and torques the two particles exert on each other as a whole, are calculated from atomic interaction potentials. As a prototype short-range potential we choose a truncated Lennard-Jones pair potential, where up to 4th nearest neighbors are taken into account. The binding energy of an atom is calculated by summing up the interaction energies with all atoms within this neighborhood, irrespective of the lattice they reside on. Likewise, the force and torque one particle exerts on the other are obtained by summing the interaction forces, respectively, torques of those pairs of atoms, where the partners belong to different particles.

For the results presented here, we created initial particles with a radius of 8 length units which consist of 3050 atoms. The atomic mass, which is needed for the integration of the rigid particle motion, is chosen to be $m=59$ atomic mass units. The units of energy and k_B times temperature are given by our choice of the parameter $\epsilon=0.2$ eV in the Lennard-Jones potential. The parameter E_0 entering the activation energy in Eq. (3) was chosen equal to ϵ. The temperature we used was $T=800$ K. It is known that the bulk melting point of a Lennard-Jones system is about 0.69 in reduced units.[28] This corresponds to 1650 K for $\epsilon=0.2$ eV. Using a simple molecular dynamics simulation we confirmed that the clusters do not start melting even at $T=1000$ K.

Another empirical parameter is the attempt frequency that appears in the Arrhenius law. We assume a constant value of $\nu_0=10^{13}$ s^{-1}, which is of the order of the Debye frequency and allows us to state the time in seconds. Time discretization with $dt=10^{-13}$ s is used for integration of the continuous particle motion.

The beginning of the system's evolution, i.e., the reorientation phase, was simulated using the hybrid KMC+RBD method. Within this regime particles in most cases adopted a persistent orientation, manifested by the development of a sinter neck. This reorientation phase comprised approximately 60 000 diffusion steps. After that the RBD-reorientation dynamics was turned off, and the lattices were fixed at their current position. This procedure corresponds to the fact that the grown sinter neck suppresses any further relative movement of the particles. The kinetic Monte Carlo diffusion, however, advanced in the same manner. Hereby we were able to significantly enhance the simulation performance for the subsequent coalescence process.

B. Transmission electron microscopy

For the complementary experimental study, we applied *in situ* transmission electron microscopy at elevated temperatures to obtain insights into the sintering behavior of loose aggregates of oxide (here: ITO) particles, which were prepared as self-supporting films. ITO is stable in the electron beam (e-beam) due to its high conductivity; evaporation of the material into the vacuum of the TEM does not play a role even at elevated temperatures.

The ITO nanoparticles were synthesized in a co-precipitation process from chloride precursors in the laboratories of our cooperation partner, Evonik Degussa GmbH. The process includes a reducing treatment of the ITO. The nanoparticles crystallized in the cubic bixbyite structure. No other phases were observed, verified by x-ray powder diffraction, synchrotron powder diffraction, as well as by high-resolution transmission electron microscopy. The initial particles were monocrystalline. These complementary measurements of the same batch of the ITO nanopowder are published in Ref. 29.

Diluted ethanol-based dispersions of the nanoparticles were dropped onto standard 400 mesh copper TEM grids to form self-supporting films stabilized by adhesion. After the solvent had evaporated, the samples were cleaned within an oxygen plasma for 3 min in order to produce clean particle surfaces.

A water-cooled double tilt hot-stage holder (Gatan Inc., type 652) was used for the experiments. The actual sample temperature is estimated to be within ± 50 K of the thermocouple temperature. A set of more than 10 different hot-stage experiments with heating rates between 5 and 25 K/min were carried out. Usually, the target temperature was set to 1170 K. For only one experiment, the target temperature was set to

1370 K. Also at this high temperature, the principal mechanism of the nanoparticle rotations could be observed. At this high temperature the copper mesh alloyed with the tantalum holder, but did not melt. So the actual sample temperature was still slightly below the copper melting temperature. The experiments were continuously monitored using a TV rate camera system equipped with a hard disk recording unit. The time resolution of two subsequent frames was 1/25 s.

The heating experiments were performed using a FEI Tecnai F20 ST or a Philips CM20. During the heating, we used a magnification of 50–90 k. This way, it was possible to correct manually for the drift of the sample in the x-y plane, as well as the focus, so that continuous observation was possible both during the heating ramp, as well as at the constant target temperature.

After the heating procedure we routinely investigated the sintered sample in high resolution at room temperature. Besides the characterization of the formed interfaces, we thereby also checked that no contamination (e.g., copper) had occurred.

III. RESULTS

A. Simulation of the coalescence of two nanoparticles

We produced an ensemble of 256 simulation runs and analyzed them systematically. During each simulation the radius of gyration R_g and the relative orientation of both particles are measured. R_g^2 is the average squared distance of atoms from the center of mass and is minimal for a sphere. It is applied to assess the stage of the coalescence process. In order to characterize the relative orientation of the clusters, a parametrization with a rotation axis and the corresponding angle is used.

Our simulations confirm that the time evolution of a soft agglomerate of two particles generally does not start with the growth of a neck between them because there are no favorable binding sites for the diffusing atoms. The two particles change their orientation relative to each other in discontinuous steps due to mutual torques (see Fig. 2). When a configuration is found that supports neck growth, the particle pair converts into a hard agglomerate. Any further reorientation becomes impossible then [cf. Fig. 1(b)–1(d) and the supplementary video sequence].[27]

Correspondingly two characteristic regimes can be distinguished, a reorientation and a coalescence phase. For the particle sizes considered in the simulation the reorientation is much faster than the coalescence. Note that the value of the radius of gyration does not change significantly, while the misorientation parameters change drastically [Fig. 2(a)] during the first regime.

The orientations adopted at the end of the reorientation phase were statistically analyzed classifying them in terms of the well-established CSL model.[12] The 256 simulation results split up into three groups: (i) 86 configurations could undoubtedly be assigned to a $\Sigma \leq 63$. (ii) 81 configurations adopted a fixed orientation, which we could not interpret within the CSL model (for $\Sigma \leq 63$). (iii) In the remaining 89 cases no fixed orientation was established within the simulated time, which means that the particles were still rolling on each other at the end of the hybrid simulation regime.

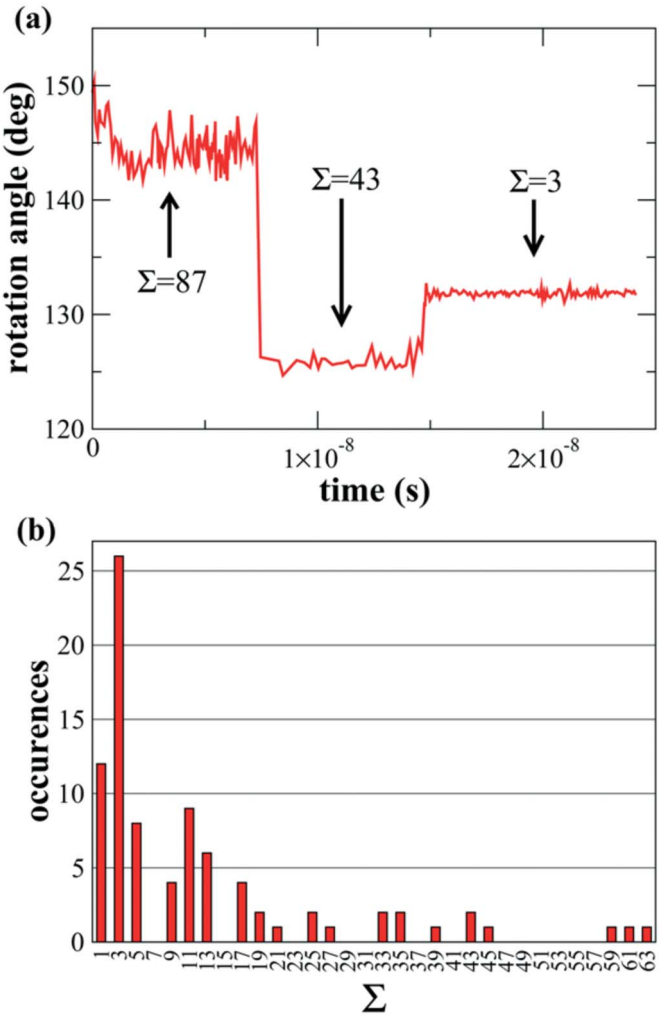

FIG. 2. (Color online) (a) A typical time evolution of the relative rotation angle around a certain fixed axis. The reorientation is discontinuous and gets stuck in some (meta)stable states. If more than one reorientation occurs, there is a trend towards lower Σ values. (b) Using the CSL model (Ref. 12) we were able to classify the finally adopted constellations for most of our runs by the CSL parameter Σ. The histogram shows the distribution of Σ values produced by 256 simulations of the same system with randomly chosen starting orientations. $1/\Sigma$ is the fraction of lattice points that coincide in both lattices. $\Sigma=1$ means the absence of any grain boundary, twin boundaries have $\Sigma=3$.

The histogram of the identified Σ orientations is given in Fig. 2(b). The histogram shows a general tendency that higher Σ values are less favorable. This can be explained because the amount of coincidence $1/\Sigma$ is a measure for the maximum possible areal density of atoms in a grain boundary between the two orientations and, hence, for the number of potential growth sites for the incipient neck. The pronounced peak at the $\Sigma=3$ orientation expresses that the twin boundary is the most probable constellation. It has been observed that several subsequent reorientation events are possible [Fig. 2(a)]. In that case, the Σ value decreases stepwise with every reorientation.

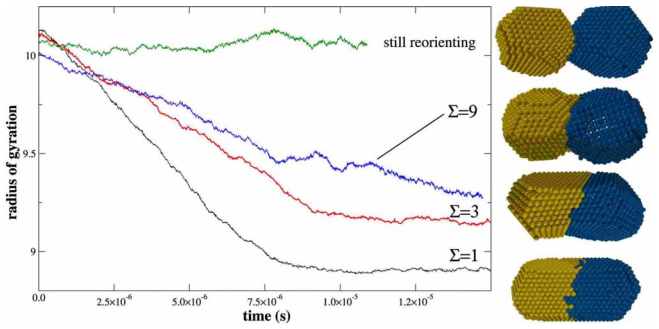

FIG. 3. (Color online) Temporal evolution of the squared radius of gyration, measured in nearest-neighbor distances, for three favorite Σ boundaries. For comparison, the corresponding curve of a system still in the discontinuous reorientation regime is added. Right: Snapshots of the simulated particle pairs each at the end of the run.

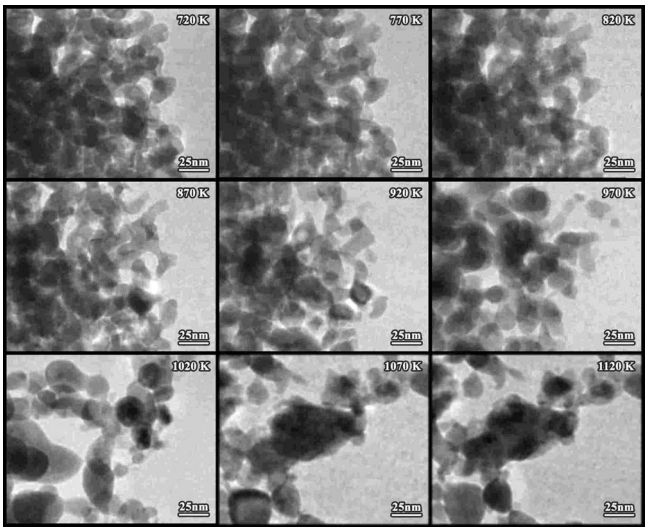

FIG. 4. Characteristic changes of the nanoparticulate film upon heating. The images present the morphology evolution in temperature steps of 50 K. The morphology of the initial self-supporting film is observed for temperatures above 720 K. The changes in morphology up to 920 K are attributed to surface diffusion, no densification is observed. At temperatures exceeding 970 K, the structure coarsens due to orientation-sensitive sintering processes. Reference 27 shows such a dynamic heating in fast motion.

The radius of gyration starts shrinking more or less rapidly depending on the final misorientation of the two lattices after a suitable orientation is found (see Fig. 3). If the system could attain the identical orientation of both lattices–which means the absence of any grain boundary–the well-known sintering laws[4] are reproduced accurately. However in many cases a complete coalescence was inhibited by a grain boundary so that the system remained dumbbell-like until the end of the simulation. As far as particle coalescence is concerned, there is a clear dependence on the Σ orientation: The smaller Σ, the faster the coalescence. This is illustrated in Fig. 3, where the temporal evolution of the radius of gyration is plotted for different values of Σ. Additionally, one representative of group (iii) (where no fixed lattice orientation was obtained) is presented. Clearly, sintering is inhibited in that case.

The relative orientation of the particles' lattices does not yet provide a complete description of a grain boundary in general. There is an additional freedom in the orientation of the grain-boundary plane, which by no means has to be perpendicular to the symmetry axis of the initial configuration of the two spherical particles. Whether complete coalescence occurs or an equilibrium shape is dumbbell-like depends on the symmetry of the interfacial plane and not just on the value of Σ.

B. *In situ* transmission electron microscopy study on the coalescence of nanoparticles

The relevance of the above-presented simulations becomes evident by a comparison with a complementary experimental study of the sintering of nanoparticles. For this purpose, we applied *in situ* transmission electron microscopy at elevated temperatures to obtain insights into the sintering behavior of loose agglomerates of oxide (here: ITO) particles.

The morphological evolution of the sample was observed and recorded between room temperature and a maximum of 1120 K. The characteristic changes upon heating are presented in Fig. 4 in steps of 50 K. The live streams of the recorded experiments are presented in the supplementary online material.[27] No change in sample morphology was observed up to temperatures of approximately 720 K. The irregular particle shape is seen; an average particle size is estimated to 10 nm, in good agreement with the macroscopic average diameter of 9.1 nm obtained from x-ray peak shape analysis according to Scherrer. Between 720–770 K the particle shape changed noticeably. A pronounced faceting of the particles is observed, giving a clear indication that surface diffusion processes become relevant on the experimental time scales. Upon rising temperatures, the particle morphology changes gradually to a less pronounced faceting and rounded particle edges at temperatures above 920 K. A change in the average particle size was first observed at 970 K, demonstrating an onset of coalescence processes just below this temperature. Thus, the coalescence processes occurred at temperatures lower than 1/2 of the bulk melting temperature (which is around 2170 K, depending on the tin content). An increasing average particle size was observed up to 1070 K; between 1070 and 1120 K no further changes occurred in the observed sample area.

The coalescence of particles was preceded by rotational movements. At increasing temperatures, these movements intensified. Events of coalescence without any preceding reorientation have hardly been observed. Yet, it was striking that at a constant temperature even as high as 1320 K, no changes in the morphology of the sample were observed. We conclude that the particles find a steady-state position after a short time at an elevated temperature and freeze then within this position. Thus, the dynamic processes of the sintering are best observed not at a constant target temperature but during the heating procedure. The rotational movement of particles, which have boundaries, contact points, or contact faces with more than one other particle so that their mobility is restricted, is hence triggered by heating.

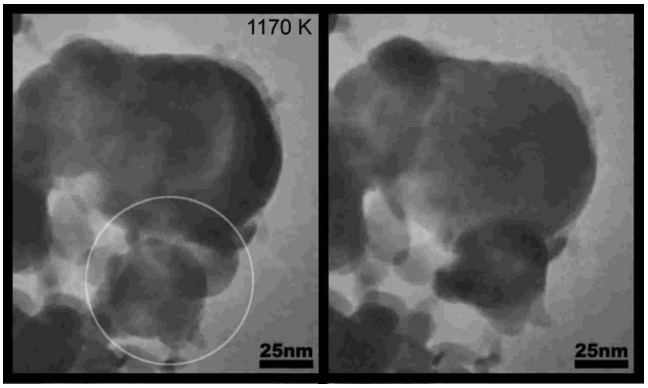

FIG. 5. One particle with a diameter of approximately 50 nm merges with another particle of a diameter of approximately 25 nm, seen at 1170 K. The coalescence was triggered by applying a fixed heating ramp. The rotational movement of the 50-nm particle was traced via the small co-rotating attached nanoparticles and the irregular shape of the agglomerate. Rotational movements prior to coalescence are shown in the movie (Ref. 27).

The reorientation of two particles is shown exemplarily in Fig. 5 and the corresponding video.[27] The actual coalescence process was faster than 1/25 s in most cases. Exceptions were found for large particles with diameters of approximately 100 nm. Also the coalescence of these comparably large particles was preceded by small reorientational movements. Thus, the principle mechanism of the nanoparticle coalescence found in our simulations—namely, that only particles with fitting orientation merge—could experimentally be verified even for particles as large as 100 nm.

In order to obtain a deeper insight into the steady state at constant temperatures, experiments were interrupted at 1000 and 1120 K. Due to a rapid cooling rate, the actual stage of the sintering was frozen and could be investigated in high resolution at room temperature. Figure 6(a) shows two particles of a diameter of less than 10 nm, which are attached to a bigger one. Their lattice orientations do not match. No indications for an ongoing sintering process, e.g., a sinter neck, are found. We observed several of those loosely attached particles, *in situ* as well as *ex situ*. Such frustrated interfaces correspond to the result of the simulations that for certain constellations of lattice misorientation, sintering is completely suppressed even at elevated temperatures.

Figure 6(b) shows a Σ boundary (apparently a twin boundary) between two adjacent particles; the (211)-lattice planes are tilted 29.2(2)° against each other. Comparable planar boundaries are often found in the *in situ* experiments. Figure 6(c) gives the impression of an interrupted coalescence process of two particles with matching orientations. The contour, which is obviously far from the thermal equilibrium shape, still gives an idea of the original sizes and shapes of the constituent particles.

While all of our observations presented above show very good agreement between simulation and experiment, the following finding seems to be at odds with our simulations at first sight: Fig. 7 shows the discontinuous, apparently free rotation of a particle between three different positions (see also supplementary material[27]). The full sequence has a length of approximately 2 s, yet each rotational step takes less than one frame, i.e., less than 1/25 s. During the time of observation no coalescence process had occurred yet. According to our simulations, however, the time scale in which a freely rotating particle of this size finds an orientation favorable for coalescence is extrapolated to be of the order of microseconds. A possible explanation for this discrepancy is that in fact the experimental particle was not freely moving, but was sterically hindered by additional particles nearby. Hence, the favorable positions may have been inaccessible. The experimental finding that no coalescence occurs can, therefore, be reconciled with the simulation.

IV. DISCUSSION

For several reasons tin-doped indium oxide nanoparticles proved to be an ideal model system for a comparison with

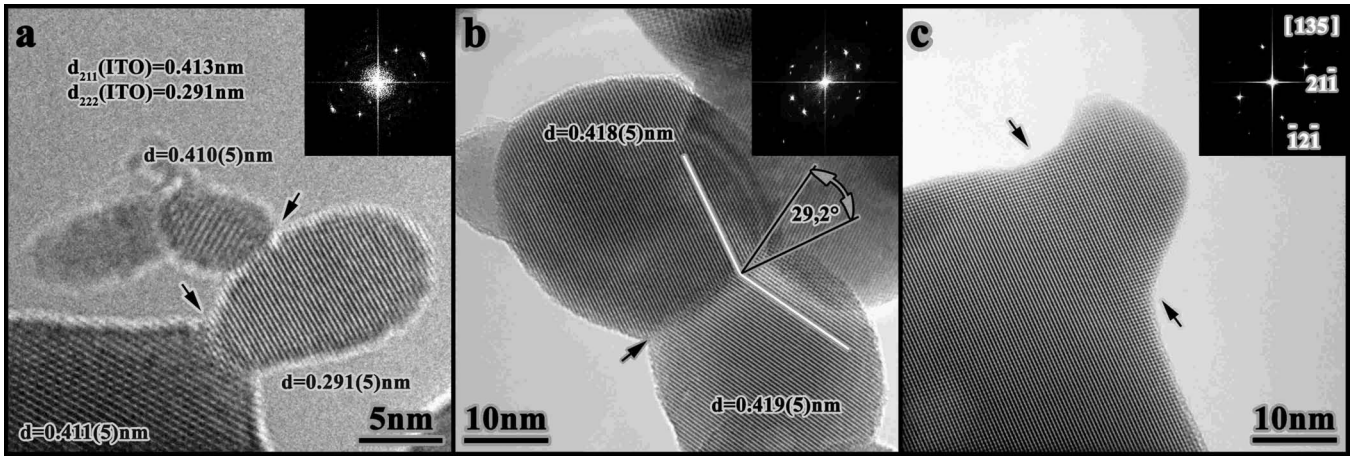

FIG. 6. Interrupted and rapidly cooled sintering experiments were postcharacterized in high-resolution at room temperature to obtain information about the lattice orientation of typical sintering stages. (a) A small particle is attached to a bigger one without matching orientation. Here, no coalescence was possible up to the temperature of 1120 K at which we interrupted the experiment. (b) Two particles have sintered together by building a Σ boundary (apparently a twin). (c) Two particles have sintered together, the orientation is completely matching, but the shape of the former constellation is still preserved.

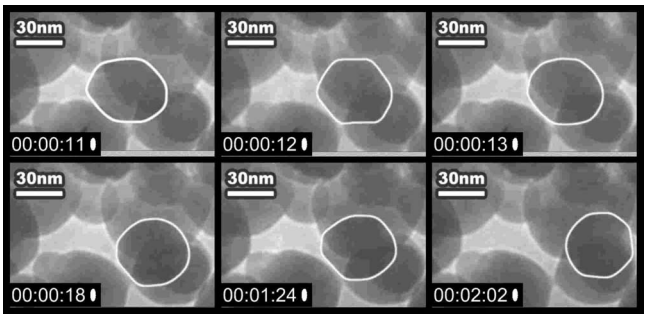

FIG. 7. The series of screenshots shows one single particle moving from one position to the next without any sintering or coalescence. The whole sequence has a length of approximately 2 s (cf. Ref. 27) and was seen at a temperature between 1120 and 1170 K. According to our simulations, the actual coalescence should occur within microseconds or less. Thus, this sequence demonstrates that unfavorable conditions, e.g., steric hindrance, suppress the sintering effectively, even though a movement of the particle was possible.

our simulations. First of all they form soft agglomerates because they were produced wet chemically. This fact is essential for being able to shed light on the initial stages of sintering. Inspecting hundreds of the initial particles in high-resolution TEM we did not find any twin boundaries, justifying the use of single-crystal particles in the simulation. During coalescence, twins and other coincident interfaces developed at the particle contacts, but migration of these defects does not play a role.

For the simulations, one fundamental assumption was made, namely, that the atoms' positions are restricted to the regular sites of the underlying lattices. In ionic crystals, the lattice positions are defined by the Coulomb forces of the ions. Therefore, cations can only assess the lattice sites of cations, anions only those of anions. The freedom within the movement of the ions within an ionic lattice is, hence, restricted, and the formation of defects such as stacking faults or dislocations upon sintering is unlikely. Therefore, the important mechanisms of the coalescence were correctly captured by the simulation. However, the complex elementary cell of ITO and the considerably bigger size of the particles, as well as the presence of more than two particles, distinguish the experimental study from the theoretical one.

Yeadon *et al.*[15] have demonstrated that copper particles only reoriented if smaller than approximately 10 nm by the crystallite rotation technique. Similar results were obtained by Ashkenazy *et al.*[17] in MD simulations. Using self-supporting films of loosely attached oxide nanoparticle, we did not see such a restriction in the length scale. The large range of experimentally observed particle sizes allows the conclusion that the theoretically predicted mechanisms remain valid for particles as large as 100 nm.

The coalescence process is preceded by particle rotations—in both experiment and simulation. In the experiments, where many-particle agglomerates are considered, the motion of one particle relative to the others is generally limited, e.g., by steric hindrance. Thus not always a position favorable for sintering can be found. In most experimental cases it is observed that the whole network morphology changes locally prior to sintering.

In the simulations, the driving forces for the rotations are the interatomic forces between the different particles. In the experiment, it is not completely clear what initiated the reorientation. For instance the sequence in Fig. 7 shows that a particle may remain at the same position for considerable time (in the 0.1 s range) until it moves again. One can conclude that such a position was not favorable for sintering. Otherwise coalescence would have occurred on this time scale. Instead, the positions were stabilized by several contacts with other particles. The point-contact binding energies are of the same order of magnitude as the thermal energy. Therefore, the particle could escape from its local potential minimum.

If not sterically hindered, a perfect alignment of the ITO particles or twin-boundary configurations is reached in most cases, leading to complete coalescence. In all other cases a dumbbell shape was adopted with a grain boundary in between. A whole variety of those boundaries can be seen in the supplementary videos.

In the simulation, only two-particle agglomerates were considered. Sterical hindrance, therefore, did not play a role. Nonetheless, we found constellations in which no coalescence occurred within the time of the simulation. This compares best with the small attaching ITO particles seen in high-resolution TEM after interrupted heating experiments (compare Fig. 6). As the orientation of the particles did not match, the small particles could not merge with bigger ones even though the surface free energy would be considerably reduced by such a ripening.

Finally, it should be mentioned that the coalescence behavior is dependent on the material and the boundary conditions of the experimental study. For ITO nanoparticles, the onset temperature of the grain coarsening depends on the surrounding atmosphere: In a complementary set of experiments we have studied the temperature-induced grain coarsening of ITO nanoparticles of the same batch by *in situ* x-ray diffraction under ambient atmosphere and evaluated the diffractograms by a peak shape analysis according to Scherrer. Grain growth started between 820 and 1020 K (compare supplementary online material[27]). Under the ultrahigh vacuum (UHV) conditions of the *in situ* TEM study, the temperature window was identified in the same region. If, on the other hand, hydrogen is added, a different surface chemistry leads to grain growth already below 570 K or even to the reduction in $In_2O_3:Sn^{4+}$ to metallic indium at moderate conditions.[29]

Not all nanoparticle materials show the same coalescence mechanism as explored in this article. Ductile materials such as metals are known to deform plastically upon first contact such that a hard agglomerate may result. A reorientation may then require the movement of dislocations[20] or the migration of stacking faults (own work under preparation). Silicon particles have neither reoriented by rotation nor by the movement of crystallographic defects but remained in their original position until the melting temperature of the whole agglomerate was reached.[30]

Our study gives an explanation of the fact that ITO is a "bad-sintering" material. Technical applications for ITO nanoparticles include, e.g., the printing of ITO dispersions as an alternative structuring method for transparent conducting

electrodes. It has been shown recently that although the electrical contact between ITO nanoparticles can be improved greatly by a temperature treatment, the porosity of layers made from ITO nanoparticles hardly decreases up to sintering temperatures of 1270 K.[31] Our interpretation is that this is because stable interfaces have built between neighboring particles that slow down further densification. This might, on the other hand, also be a chance: The compaction of nanopowder to bulk material while preserving the special nanoproperties is often hindered by the coarsening of the nanoparticles. The use of or the addition of bad-sintering oxides might slow down this process.

V. CONCLUSION

In a combined experimental and theoretical study we found the following coalescence characteristic of single-crystalline, nonmetallic particles:

(1) The theoretical model predicts a lattice reorientation prior to the coalescence process. A classification of sintered particle pairs was done using the coincidence-site-lattice (CSL) theory. The most probable constellation was a twin boundary ($\Sigma=3$) between the former particles.

(2) The smaller the Σ value adopted during the time of reorientation, the faster the following sintering of the two particles, monitored by the shrinkage of the radius of gyration. Higher Σ values lead to a dumbbell-like shape of the sintered hard agglomerate.

(3) Not all simulated particle pairs found a suitable orientation for coalescence in the simulated time. Sintering is then suppressed.

(4) Reorientational movements also preceded the coalescence of indium tin oxide nanoparticles in the hot-stage experiments as predicted by the simulation. Because agglomerates of more than two particles were observed, small reorientations resulted in considerable changes of the thin film morphology.

(5) Interrupted heating experiments demonstrated the occurrence of perfectly aligned particles, particles with twin boundaries, as well as nonsintered particles, which are misaligned, in accordance with the simulation.

(6) The principles of the coalescence did not change for all experimentally studied particles. As a huge variety of particle diameters could be observed by TEM, the theoretical model could be substantiated not only for small particles (<10 nm), but also for particles with a diameter of around 100 nm. This is a diameter range which is theoretically hard to capture because of limited calculation time.

ACKNOWLEDGMENTS

We acknowledge the dispersions and inks containing nanoparticles of ITO provided by the Degussa Evonik GmbH, as well as financial support within the frame of the projects of the Nanotronics Science-to-Business Center, financially supported by the state of North-Rhine Westphalia and co-financed by the European Union. Helpful discussions with R. Schmechel and with F. Westerhoff are gratefully acknowledged. This work was supported by German Research Foundation (DFG) through Contract No. SFB 445: Nanoparticles from the gas phase.

*dietrich.wolf@uni-due.de

[1] I. W. Chen and X. H. Wang, Nature (London) **404**, 168 (2000).
[2] J. R. Groza, Nanostruct. Mater. **12**, 987 (1999).
[3] S. Tsantilis and S. E. Pratsinis, Langmuir **20**, 5933 (2004).
[4] F. A. Nichols and W. W. Mullins, J. Appl. Phys. **36**, 1826 (1965).
[5] W. Koch and S. K. Friedlander, J. Colloid Interface Sci. **140**, 419 (1990).
[6] B. J. Kellett and F. F. Lange, J. Am. Ceram. Soc. **72**, 725 (1989).
[7] F. F. Lange and B. J. Kellett, J. Am. Ceram. Soc. **72**, 735 (1989).
[8] M. Ke, S. A. Hackney, W. W. Milligan, and E. C. Aifantis, Nanostruct. Mater. **5**, 689 (1995).
[9] K. E. Harris, V. V. Singh, and A. H. King, Acta Mater. **46**, 2623 (1998).
[10] C. S. Nichols, C. M. Mansuri, S. J. Townsend, and D. A. Smith, Acta Metall. Mater. **41**, 1861 (1993).
[11] T. Yamasaki, Y. Demizu, and Y. Ogino, *Grain Growth in Polycrystalline Materials II* (Transtec Publications LTD, 1996), Vol. 204, Pts. 1 and 2, pp. 461–466.
[12] W. Bollmann, *Crystal Defects and Crystalline Interfaces* (Springer-Verlag, Berin, 1970).
[13] S.-W. Chan and R. W. Balluffi, Acta Metall. **33**, 1113 (1985)
[14] S.-W. Chan and R. W. Balluffi, Acta Metall. **34**, 2191 (1986)
[15] M. Yeadon, J. C. Yang, R. S. Averback, J. W. Bullard, D. L. Olynick, and J. M. Gibson, Appl. Phys. Lett. **71**, 1631 (1997).
[16] J. K. Bording, B. Q. Li, Y. F. Shi, and J. M. Zuo, Phys. Rev. Lett. **90**, 226104 (2003).
[17] Y. Ashkenazy, R. S. Averback, and K. Albe, Phys. Rev. B **64**, 205409 (2001).
[18] S. Arcidiacono, N. R. Bieri, D. Poulikakos, and C. P. Grigoropoulos, Int. J. Multiphase Flow **30**, 979 (2004).
[19] H. L. Zhu and R. S. Averback, Philos. Mag. Lett. **73**, 27 (1996).
[20] R. W. Balluffi, A. Brokman, and A. H. King, Acta Metall. **30**, 1453 (1982).
[21] J. Rankin, J. Am. Ceram. Soc. **82**, 1560 (1999).
[22] J. Rankin and B. W. Sheldon, Mater. Sci. Eng., A **204**, 48 (1995).
[23] A. B. Bortz, M. H. Kalos, and J. L. Lebowitz, J. Comput. Phys. **17**, 10 (1975).
[24] L. Kantorovich, Phys. Rev. B **75**, 064305 (2007).
[25] N. S. Martys and R. D. Mountain, Phys. Rev. E **59**, 3733 (1999).
[26] D. C. Rapaport, *The Art of Molecular Dynamics Simulation* (Cambridge University Press, Cambridge, 1995).
[27] See EPAPS Document No. E-PRBMDO-78-102840 for supplementary online material which contains videos to Figs. 1, 4, 5, and 7. They show a simulation of the sintering process, morphological changes upon heating of the ITO film, particle rotation prior to the merging, and the movement of a single particle. The supplementary online material also contains additional ITO *in situ* x-ray data. For more information on EPAPS, see http://www.aip.org/pubservs/epaps.html.

[28] Ethan A. Mastny and Juan J. de Pablo, J. Chem. Phys. **127**, 104504 (2007).
[29] G. Guenther, G. Schierning, R. Theissmann, R. Kruk, R. Schmechel, C. Baehtz, and A. Prodi-Schwab, J. Appl. Phys. **104**, 034501 (2008).
[30] G. Schierning, R. Theissmann, H. Wiggers, D. Sudfeld, A. Ebbers, D. Franke, V. T. Witusiewicz, and M. Apel, J. Appl. Phys. **103**, 084305 (2008).
[31] M. Gross, A. Winnacker, and P. J. Wellmann, Thin Solid Films **515**, 8567 (2007).